

Experimental Tests Of Paleoclassical Transport

J.D. Callen¹, J.K. Anderson¹, T.C. Arlen^{2,3}, G. Bateman⁴, R.V. Budny⁵, T. Fujita⁶, C.M. Greenfield³, M. Greenwald⁷, R.J. Groebner³, D.N. Hill³, G.M.D. Hogewij⁸, S.M. Kaye⁵, A.H. Kritiz⁴, E.A. Lazarus⁹, A.C. Leonard³, M.A. Mahdavi³, H.S. McLean¹⁰, T.H. Osborne³, A.Y. Pankin⁴, C.C. Petty³, J.S. Sarff¹, H.E. St. John³, W.M. Stacey¹¹, D. Stutman¹², E.J. Synakowski¹⁰, K. Tritz¹²

¹University of Wisconsin, Madison, WI 53706-1609 USA

²California Polytechnic State University, San Luis Obispo, CA 93407 USA

³General Atomics, San Diego, CA 92186-5608 USA

⁴Lehigh University, Bethlehem, PA 18015-3182 USA

⁵Princeton Plasma Physics Laboratory, Princeton, NJ 08543-0451 USA

⁶Naka Site, JAEA, 801-1 Mukouyama, Naka, Ibaraki-ken, 311-0193, JAPAN

⁷Massachusetts Institute of Technology, Cambridge, MA 02139 USA

⁸FOM Institute for Plasma Physics Rijnhuizen, 3430 BE Nieuwegein, NETHERLANDS

⁹Oak Ridge National Laboratory, Oak Ridge, TN 37831 USA

¹⁰Lawrence Livermore National Laboratory, Livermore, CA 94551-0808 USA

¹¹Georgia Tech, Atlanta, GA 30332 USA

¹²Johns Hopkins University, Baltimore, MD 21218 USA

e-mail, webpage of main author: callen@engr.wisc.edu, <http://homepages.cae.wisc.edu/~callen>

Abstract. Predictions of the recently developed paleoclassical transport model are compared with data from many toroidal plasma experiments: electron heat diffusivity in DIII-D, C-Mod and NSTX ohmic and near-ohmic plasmas; transport modeling of DIII-D ohmic-level discharges and of the RTP ECH “stair-step” experiments with eITBs at low order rational surfaces; investigation of a strong eITB in JT-60U; H-mode T_e edge pedestal properties in DIII-D; and electron heat diffusivities in non-tokamak experiments (NSTX/ST, MST/RFP, SSPX/spheromak). The radial electron heat transport predicted by the paleoclassical model is found to agree with a wide variety of ohmic-level experimental results and may set the lower limit (within a factor ~ 2) on the radial electron heat transport in most resistive, current-carrying toroidal plasmas — unless it is exceeded by fluctuation-induced transport, which often occurs in the edge of L-mode plasmas and when the electron temperature is high ($\gtrsim T_e^{\text{crit}} \simeq B^{2/3} \bar{a}^{1/2}$ keV) because then paleoclassical transport becomes less than gyro-Bohm-level anomalous transport.

1. Introduction

A new model for an irreducible minimum level of radial electron heat transport, the paleoclassical model, was introduced at the 2004 IAEA Vilamoura meeting [1a]; its basic features [1b] and details [1c] are now published. The key hypothesis of the model is that in resistive, current-carrying toroidal plasmas electron guiding centers diffuse radially with thin annuli of poloidal magnetic flux on the magnetic (“skin”) diffusion time scale. This key hypothesis was originally motivated phenomenologically [1c]; recently, a derivation of it has been developed [2]. This paper carries the initially encouraging comparisons with experimental data [1a] to a higher level via a number of more detailed comparisons of paleoclassical electron heat transport with data from a variety of toroidal plasma experiments. It also seeks to determine the situations (mainly ohmic-level plasmas and in the cooler plasma edge) where paleoclassical radial electron heat transport is dominant. Most comparisons are with well-characterized, previously published experimental data. In general, “typical best case” comparisons are shown in the figures; the text comments on other comparisons and on some cases where the paleoclassical model does not represent the experimental data well. The main comparisons are between the radial electron heat diffusivities predicted by the paleoclassical model and those inferred from “power balance” analyses; since typical error bars in both the theory [1] and experimental data analysis are of order a factor of two, agreement within this margin will be considered satisfactory. Some dynamic modeling tests are also presented.

2. Brief Summary Of Paleoclassical Model

The paleoclassical radial electron heat transport to be added to the right of an electron energy balance equation, and the implied radial electron heat diffusivity χ_e^{pc} and magnetic field diffusivity D_η are [1a,1c]

$$-\langle \nabla \cdot \mathbf{Q}_e^{\text{pc}} \rangle = \frac{M+1}{V'} \frac{\partial^2}{\partial \rho^2} \left(V' \frac{\eta_{\parallel}^{\text{nc}}}{\mu_0 \bar{a}^2} \frac{3}{2} n_e T_e \right), \quad \chi_e^{\text{pc}} \equiv \frac{3}{2} (M+1) D_\eta, \quad D_\eta \equiv \frac{\eta_{\parallel}^{\text{nc}}}{\mu_0} \sim \frac{\eta_0}{\mu_0} \equiv \frac{1400 Z_{\text{eff}}}{T_e (\text{eV})^{3/2}}, \quad (1)$$

in which $\eta_{\parallel}^{\text{nc}}$ is the neoclassical parallel resistivity, the unity in $M+1$ represents the axisymmetric contribution [1c], and the helical multiplier M and average minor radius \bar{a} are [1a,1c]

$$M = \frac{\min\{\ell_{\text{max}}, \lambda_e, \ell_{n^\circ}\}}{\pi \bar{R} q} \simeq \frac{1}{\pi \bar{R} q} \frac{1}{1/\lambda_e + 1/\ell_{\text{max}}}, \quad \frac{1}{\bar{a}^2} \equiv \frac{\langle |\nabla \rho|^2 / R^2 \rangle}{\langle R^{-2} \rangle} \simeq \frac{1}{a^2} \frac{1 + \kappa^2}{2 \kappa^2}. \quad (2)$$

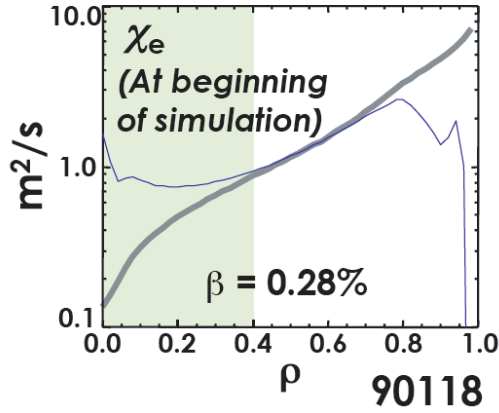


Figure 1: DIII-D electron heat diffusivity in ohmic-level beta-scan discharge: analysis (thick gray line), paleo (blue), sawtooth (shaded).

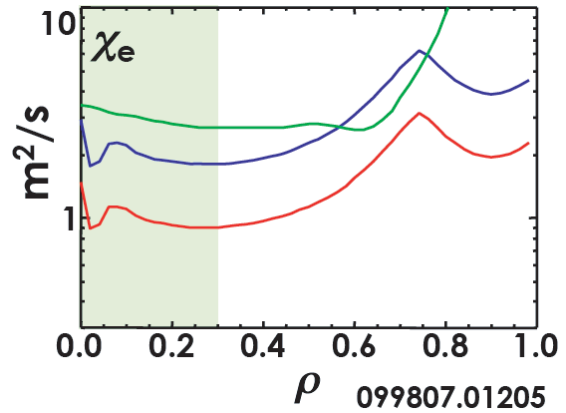


Figure 2: DIII-D electron heat diffusivity in Linear Ohmic Confinement (LOC) regime: analysis (green), paleo (red), 2×paleo (blue).

The formulas after the \simeq indicate the usually applicable smoothing formula for M and an approximate formula for elliptical cross-section plasmas with $\kappa \equiv b/a \geq 1$. Further, $\lambda_e \simeq 1.2 \times 10^{16} T_e (\text{eV})^2 / n_e Z_{\text{eff}}$ is the electron collision length and ℓ_{max} is the length over which magnetic field lines diffuse radially [1a,1c]:

$$\ell_{\text{max}} = \pi \bar{R} q n_{\text{max}}, \quad n_{\text{max}} = (\pi \bar{\delta}_e |q'|)^{-1/2}; \quad \max\{n_{\text{max}}\} = (\pi^2 \bar{\delta}_e^2 |q''|)^{-1/3}, \quad \text{when } |q'| \simeq 0. \quad (3)$$

Here, $\bar{\delta}_e \equiv c/\omega_p \bar{a}$ is the normalized electromagnetic skin depth. Paleoclassical diffusivity limits are

$$\text{collisionless}_{\lambda_e > \ell_{\text{max}}} \chi_e^{\text{pc}} = \frac{3}{2} \frac{\eta_{\parallel}^{\text{nc}}}{\mu_0} n_{\text{max}}, \quad \text{collisional}_{\ell_{\text{max}} > \lambda_e > \pi \bar{R} q} \chi_e^{\text{pc}} = \frac{3}{2} \frac{v_{Te} c^2 \eta_{\parallel}^{\text{nc}}}{\pi \bar{R} q \omega_p^2 \eta_0}, \quad \text{edge}_{\pi \bar{R} q > \lambda_e > \pi R} \chi_e^{\text{pc}} \simeq \frac{10^3 Z_{\text{eff}}}{T_e (\text{eV})^{3/2}}. \quad (4)$$

Because χ_e^{pc} scales with magnetic field diffusivity $D_\eta = \eta_{\parallel}^{\text{nc}}/\mu_0$, it scales as $\bar{a}^{1/2} T_e^{-3/2}$ in the collisionless regime and decreases as T_e increases. In contrast, drift-wave-type instabilities (ITG, DTEM, ETG) induce micro-turbulence and anomalous heat transport, which scale with the gyro-Bohm coefficient [1a] $\chi_e^{\text{gB}} \simeq f_{\#} 3.2 T_e (\text{keV})^{3/2} A_i^{1/2} / \bar{a} B^2$, that increase as T_e increases. While the coefficient $f_{\#}$ is in general not well quantified, ITG simulations often find $\chi_e/\chi_i \lesssim 1/3$ and experimental results from TCV [3] indicate $f_{\#} \lesssim 1/3$, for all R/L_{Te} . Using $f_{\#} \simeq 1/3$, we can anticipate [1a] that, roughly speaking, below some T_e ,

$$T_e \leq T_e^{\text{crit}} \simeq B(\text{T})^{2/3} \bar{a}(\text{m})^{1/2} \text{keV}, \quad \text{paleoclassical electron heat transport should be dominant.} \quad (5)$$

Thus, we explore transport comparisons mainly in lower T_e ohmic-level and edge plasmas.

3. DIII-D Confinement Region Electron Heat Transport Comparisons

Comparisons of paleoclassical predictions with $\chi_e^{\text{pb}} \equiv \langle \mathbf{Q}_e \cdot \nabla V \rangle / \langle -n_e \nabla T_e \cdot \nabla V \rangle$ experimental “power balance” analysis data are most appropriate in the confinement region of tokamak plasmas, $0.4 \lesssim \rho \lesssim 0.9$ — because sawteeth often occur for $\rho \lesssim 0.4$ and transport data typically have large uncertainties for $\rho \gtrsim 0.9$. In the confinement region, tokamak plasmas are usually in the “collisionless” paleoclassical regime [1] where ℓ_{max} dominates in (2) and $M = n_{\text{max}} \sim 10$. Comparisons of χ_e^{pc} with experimental χ_e^{pb} data from 6 of the base ohmic-level [$T_e(0.4) \lesssim T_e^{\text{crit}} \sim 1\text{--}1.35$ keV] discharges in DIII-D beta [4a] and collisionality [4b] scans show reasonable agreement [5] — similar profiles and plasma parameter scaling, and usually within a factor of about 2 in magnitude [but low by a factor ~ 3 for low collisionality where $T_e(0.4) \gtrsim T_e^{\text{crit}}$], except near the edge. A “typical best case” comparison is shown in Fig. 1. Here, χ_e^{pc} decreases toward the edge ($\rho \gtrsim 0.8$ in Fig. 1) because the collision length λ_e becomes less than ℓ_{max} and one transitions to the “collisional” (Alcator scaling) paleoclassical regime where $M = \lambda_e/\pi \bar{R} q$ and $\chi_e^{\text{pc}} \propto T_e^{1/2}/n_e q$. The increase of χ_e^{pb} with ρ there could be caused by anomalous plasma transport induced by resistive ballooning modes (RBMs) [6] in this $T_e \lesssim 300$ eV region of these ohmic L-mode plasmas.

Figure 2 shows a similar comparison for a DIII-D plasma in the Linear Ohmic Confinement (LOC) regime [7] where $\tau_E \sim n_e$ and one would expect [1] to be in the collisional (Alcator-scaling) regime; while the agreement is reasonable over the critical region (for overall energy confinement) of $0.5 \lesssim \rho \lesssim 0.8$, this

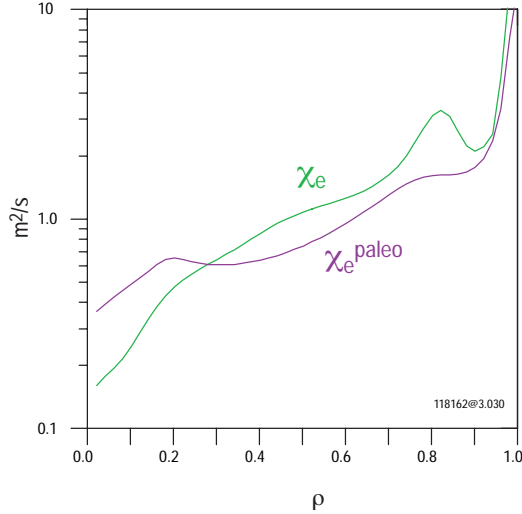


Figure 3: Profile of χ_e just before a sawtooth crash in DIII-D bean-shaped plasma [9].

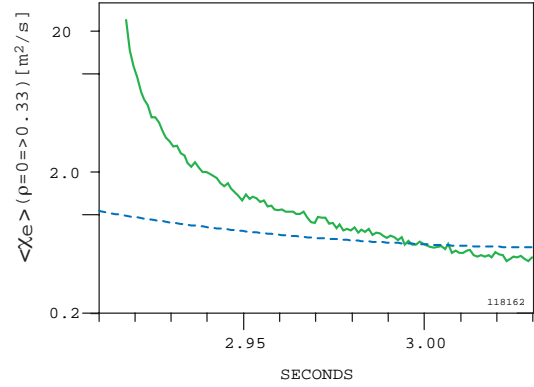


Figure 4: Average χ_e decays between sawtooth crashes: analysis (green), paleo (blue dashed) [9].

plasma is only marginally in the paleoclassical collisional regime there. A comparison in a higher density Saturated Ohmic Confinement (SOC) discharge, in which ITG turbulence was inferred to be present [7], found χ_e^{pc} to be in the right range, but with the wrong (collisional) profile over this same radial region.

Dynamic ONETWO modeling of all these DIII-D discharges (from $\rho = 0.9$ inward) using the paleoclassical transport model yields T_e profiles in reasonable agreement (within $\lesssim 20\%$) where $T_e \lesssim T_e^{\text{crit}}$. However, “thermal run away” occurs in simulations without a sawtooth model in the central, sawtoothing region $\rho \lesssim 0.4$ because the collisionless χ_e^{pc} , which is applicable there, decreases with increasing T_e .

Comparisons with DIII-D “hybrid” discharges [8] at $\rho \sim 0.5$ where $T_e \gtrsim 2.5$ keV ($\gg T_e^{\text{crit}} \simeq 1.3$ keV) show [5] that χ_e^{pc} is a factor of 5–7 too small and has a different profile from χ_e^{pb} for these discharges, which have micro-turbulence fluctuations (presumably due to ITG modes) and 3/2 NTMs in them. Thus, we conclude that for DIII-D ohmic-level plasmas the paleoclassical model predicts the χ_e magnitude and profile (\lesssim factor of 2) and T_e profile within the confinement region — as long as $T_e \lesssim T_e^{\text{crit}}$ there.

There are, however, situations in DIII-D where χ_e^{pc} sets the minimum level of transport even when $T_e \gg T_e^{\text{crit}}$. Figure 3 shows such a case; it was obtained with a bean-shaped cross-section DIII-D plasma developed for sawtooth studies [9]. At the time shown (just before a sawtooth crash) it has $T_e(0) \simeq 2.5$ keV $\gg T_e^{\text{crit}} \simeq 1.3$ keV. Also, Fig. 4 shows that the core-averaged χ_e decays down to the paleoclassical level just before the next sawtooth crash. In a corresponding oval cross-section DIII-D plasma the $\langle \chi_e^{\text{pb}} \rangle$ values were much higher earlier in time, but again decreased to $\langle \chi_e^{\text{pc}} \rangle$ just before the next sawtooth crash.

4. C-Mod Electron Heat Diffusivity, Critical T_e Gradient And Power Flow

Alcator C-Mod operates at higher magnetic field and thus has a higher T_e^{crit} — about 1.6 keV for $B \simeq 5.3$ T and $\bar{a} \simeq 0.27$ m. Figure 5 shows a comparison of χ_e^{pc} with the experimental χ_{eff} , which includes both electron and ion heat diffusivities, for a well-diagnosed H-mode discharge [10]. For this discharge sawteeth influence $\rho \lesssim \rho_{\text{inv}} \simeq 0.35$ and $T_e \lesssim T_e^{\text{crit}} \simeq 1.6$ keV for $\rho > 0.45$. Figure 5 shows χ_e^{pc} agrees well with C-Mod H-mode data in all three regimes in (4): collisionless for $\rho < 0.43$, collisional for $0.43 < \rho < 0.85$ and edge for $\rho > 0.85$. Similar agreement is also obtained for an L-mode discharge [10].

The original paleoclassical papers [1] noted that the paleoclassical electron heat transport operator in (1) naturally includes heat pinch or minimum temperature gradient effects. Their specific forms were given [1a,1c] under the assumption that $M+1$ varies little with ρ . However, M varies significantly for the C-Mod data in Fig. 5 — from ~ 15 for $\rho < 0.43$ down to < 1 for $\rho > 0.85$. Thus, attempts to compare the critical T_e gradient scale length in (58) of [1a] with the data in Fig. 5 failed, except for $\rho > 0.85$ where it should be valid (because $M+1 \sim 1$ there) and did represent the data. As a check on the form of the

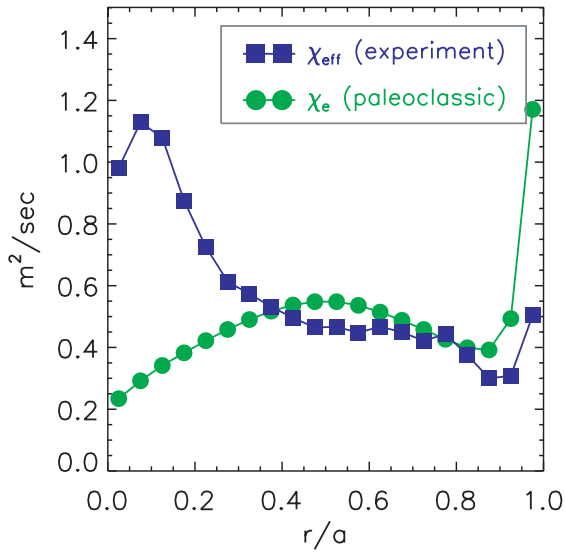


Figure 5: Electron heat diffusivity profile for C-Mod H-mode shot 960116027 [10].

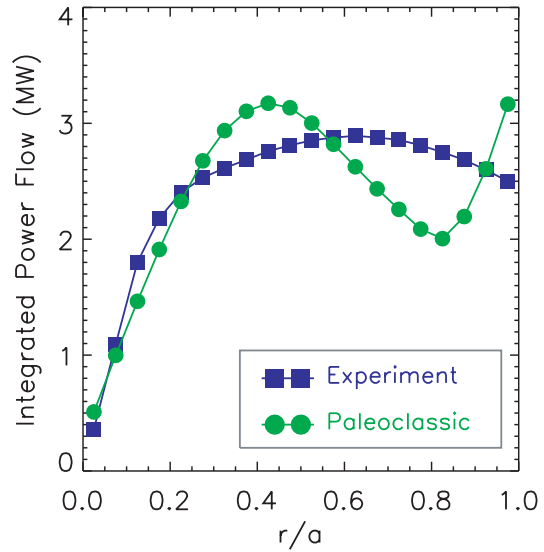


Figure 6: Radial electron power flow versus radius for C-Mod H-mode shot 960116027 [10].

paleoclassical transport operator, Fig. 6 shows that the volume integral of the first form in (1) agrees reasonably well with the experimental electron power flow for the H-mode discharge [10] in Fig. 5.

5. Electron Internal Transport Barriers (eITBs) in RTP and JT-60U

Near a low order rational surface (e.g., $q^\circ \equiv m^\circ/n^\circ = 2/1$), $\ell_{n^\circ} \equiv \pi \bar{R} q^\circ n^\circ$ dominates in (2) and $M \simeq n^\circ$, which yields [1a,1c] electron “internal transport barriers” where χ_e^{pc} is smaller by $(n^\circ+1)/n_{\text{max}} \sim 0.2\text{--}0.5$ over widths determined by magnetic shear [1], as shown in Fig. 7. These features produce transport barriers like those inferred [11] from the RTP “stair-step” experiments in which the central T_e decreased abruptly as radially highly localized ECH was moved radially outward (in steps $\lesssim 0.01 a$) past low order rational surfaces. Modeling [12] of such RTP discharges with twice χ_e^{pc} is shown in Fig. 8.

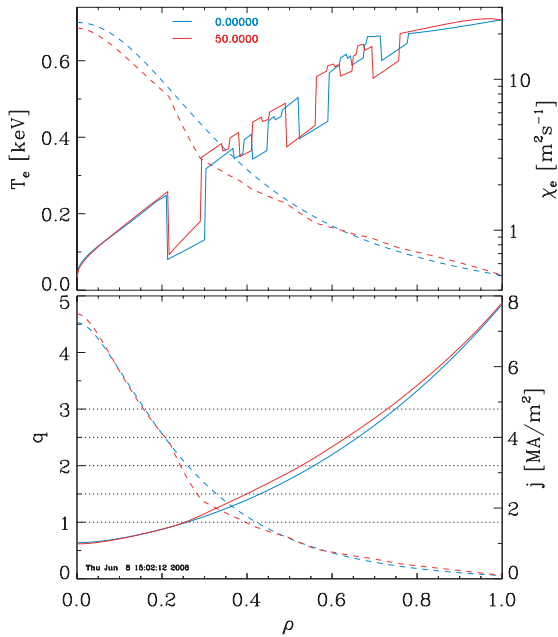


Figure 7: Profiles for RTP ohmic discharge: initially (blue, expt. T_e), pc modeling at 50 ms (red). Largest eITBs are at $q = 1/1, 2/1, 3/1$ [12].

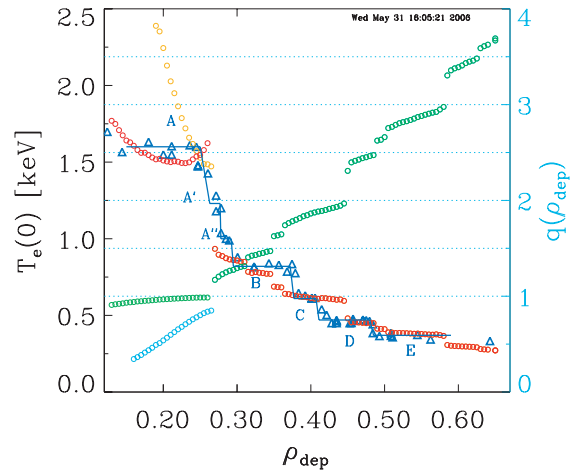


Figure 8: T_e on axis as ECH deposition is moved radially outward: RTP expt. (blue), paleo modeling (red with sawtooth model, orange w/o) [12].

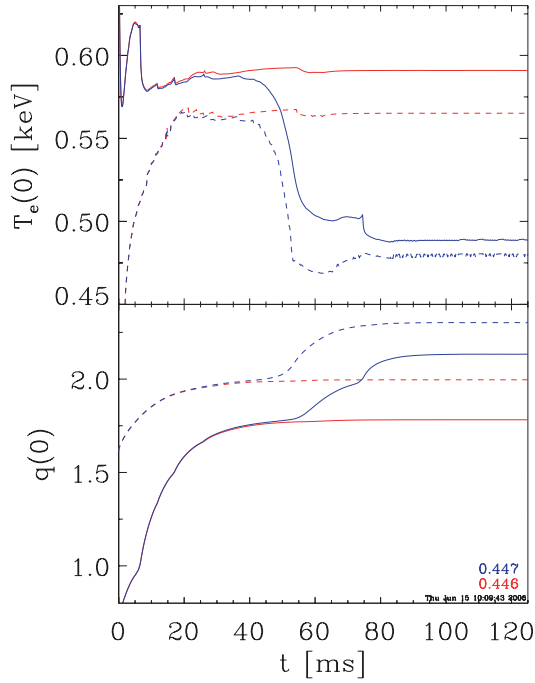


Figure 9: Evolution of central T_e , q for ECH $\rho_{\text{dep}} = 0.446$ (red), 0.447 (blue): RTP experiment (solid) and paleoclassical modeling (dashed) [12].

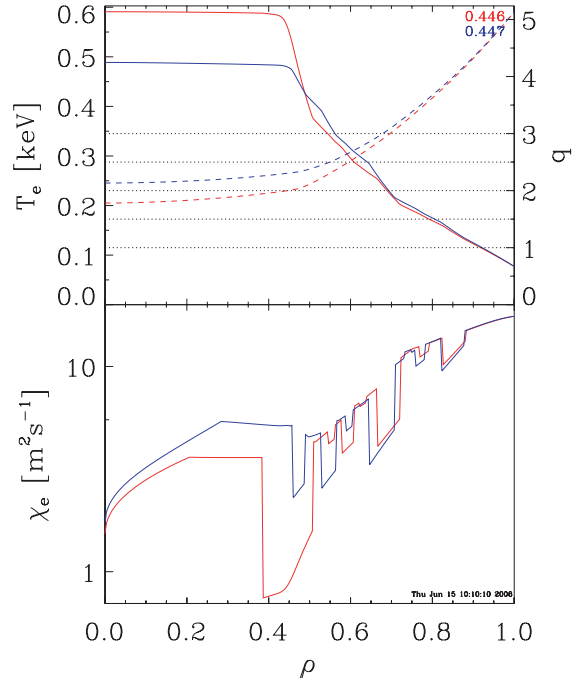


Figure 10: Corresponding paleoclassical modeling profiles of T_e , q and χ_e for ECH $\rho_{\text{dep}} = 0.446$ (red), 0.447 (blue) in RTP [12].

[With $1 \times \chi_e^{\text{pc}}$ only slightly higher $T_e(0)$ values and modified q profiles are obtained.] For most of these cases $T_e \lesssim T_e^{\text{crit}} \simeq 0.7$ keV over most of the plasma and the collisionless χ_e^{pc} is applicable for $\rho \lesssim 0.8$. The paleoclassical model results shown in Fig. 8 approximate the “stair step” details of the T_e profile reasonably well. (However, the paleoclassical model does not reproduce the slightly hollow T_e profiles that are observed experimentally for far off axis ECH which modify the barrier locations a bit [12].) As in the DIII-D dynamic modeling, “thermal runaway” occurs for $\rho \lesssim 0.25$ (orange points in Fig. 8) — unless a sawtooth T_e relaxation model is used there (red points). The presence of eITBs at low order rational surfaces requires plasmas to come into a steady equilibrium [11] — apparently on the slow magnetic diffusion time scale. Paleoclassical modeling [12] of the evolution of two RTP plasmas with very closely spaced ECH deposition radii is shown in Fig. 9. The corresponding T_e , q and χ_e^{pc} profiles are shown in Fig. 10. The position sensitivity, temporal behavior and sharp transport bifurcations are well represented by the modeling of these cases in which the magnetic field diffusion time is $\tau_\eta \equiv a^2/6D_\eta(\rho=0) \sim 20$ ms.

Similarly, the original paleoclassical papers [1] proposed that strong eITBs produced in JT-60U [13] were induced by an off-axis minimum in q occurring at a low order rational surface which could cause a small $\chi_e^{\text{pc}} \sim n^\circ D_\eta$ there. While such an effect may help initiate an eITB, it is not relevant in fully developed JT-60U eITBs. Rather, the strong reversed shear inside q_{min} decreases the collisionless $\chi_e^{\text{pc}} \sim |q'|^{-1/2}$ there. Then, if the anomalous transport due to micro-turbulence is negligible, χ_e^{pc} can produce the low, irreducible minimum level of electron heat transport. An example of this behavior for a strong eITB in JT-60U, for which $T_e^{\text{crit}} \simeq 2.4$ keV, is shown in Figs. 11 and 12. The TRANSP analysis (Fig. 12) shows that the eITB occurs primarily inside the q_{min} surface at $\rho \simeq 0.575$ and that the reduction in χ_e there is well represented by the paleoclassical model in this JT-60U discharge in which a “reduction in the size of the turbulent structures is observed ... during the evolution of the internal transport barrier” [14]. Strongly reversed magnetic shear can also be important in the core of NSTX plasmas — see 7. below.

6. H-Mode Edge T_e Pedestals in DIII-D

Figures 1, 2, and 5 show that as ρ approaches the separatrix, χ_e^{pc} is first in the collisional regime where $\chi_e^{\text{pc}} \propto T_e^{1/2}/n_e q$ decreases with increasing ρ . Further out where $\lambda_e < \pi R q$, $M < 1$ and $\chi_e^{\text{pc}} \propto T_e^{-3/2}$ increases as T_e decreases further. Edge pedestal n_e and T_e profiles are shown in Fig. 13 for a well-diagnosed DIII-D H-mode discharge with 36 ms between ELM crashes. Figure 14 shows a comparison of χ_e^{pc} with results from an integrated transport analysis code [15] of an analogous DIII-D shot 92976 which had a

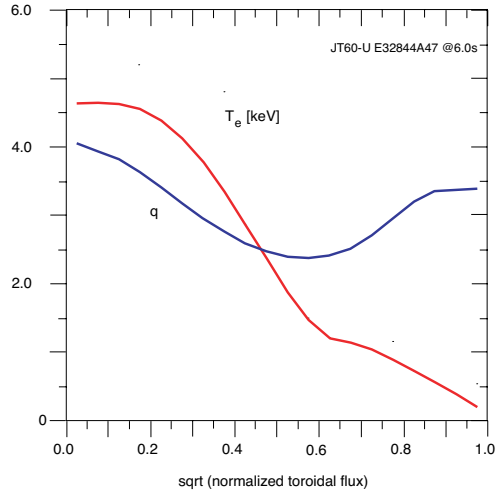


Figure 11: Profiles of T_e , q in JT-60U for a strong eITB, which is inside of q_{\min} at $\rho \simeq 0.575$.

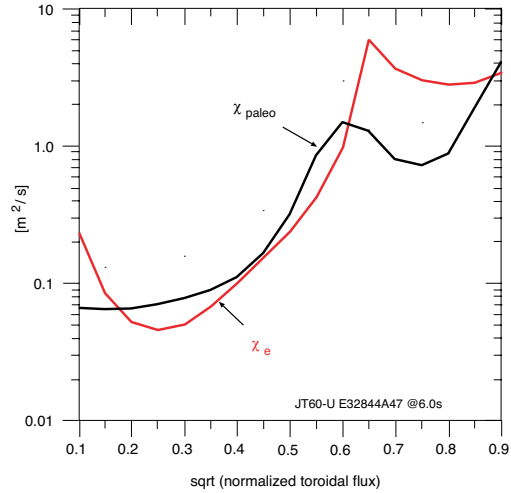


Figure 12: Comparison of TRANSP and paleoclassical χ_e for the JT-60U case in Fig. 11.

higher pedestal $n_e^{\text{ped}} \simeq 4.3 \times 10^{19} \text{ m}^{-3}$ but lower $T_e^{\text{ped}} \simeq 300 \text{ eV}$. The paleoclassical χ_e compares favorably with the experimentally inferred χ_e for most cases analyzed to date, especially in the near separatrix region ($\rho > 0.96$) where $\chi_e^{\text{pc}} \propto T_e^{-3/2}$. The increase of χ_e^{pc} with ρ in the near separatrix region causes the T_e profile to have positive or neutral curvature there (i.e., $\partial^2 T_e / \partial \rho^2 \geq 0$), for example outside the T_e “symmetry point” at $\rho = 0.978$ in Fig. 13. This aspect of the paleoclassical model is critical for producing appropriate ASTRA modeling [16] of the edge T_e pedestal, as illustrated in Fig. 15.

Paleoclassical predictions have been developed for the T_e profile in an H-mode edge pedestal region [17]. Near the separatrix $M < 1$ and $n_e T_e D_\eta \propto n_e / T_e^{1/2}$; thus, integrating the first equation in (1) from the separatrix inward the paleoclassical model predicts [17] $T_e \propto n_e^2$ or $\eta_e \equiv d \ln T_e / d \ln n_e = 2$, in agreement with ASDEX-U [18] and DIII-D data very close to the separatrix ($T_e \lesssim 200 \text{ eV}$) [17]. This relation applies up to the point ($\rho \lesssim 0.94$ in Figs. 14, 15) where $\lambda_e \gtrsim \pi R q / 2$ and $M \gtrsim 0.5$, beyond which χ_e^{pc} stops decreasing or reaches a minimum and causes a maximum $|\nabla T_e|$. Further inward, χ_e^{pc} increases into the collisional regime, but χ_e from ITG/TEM modes increases even faster (for $\rho < 0.9$ in Fig. 15). The pedestal T_e is predicted by balancing paleoclassical transport against gyro-Bohm-scaled anomalous electron heat transport, which yields a prediction of $\beta_e^{\text{ped}} \equiv n_e^{\text{ped}} T_e^{\text{ped}} / (B^2 / 2\mu_0) \simeq (0.032 / f_\# A_i^{1/2}) (\bar{a} / R q) (\eta_{\parallel}^{\text{nc}} / \eta_0)$, which is reasonably consistent with the DIII-D pedestal database for $f_\# \sim 0.6$ [17] — see Fig. 16.

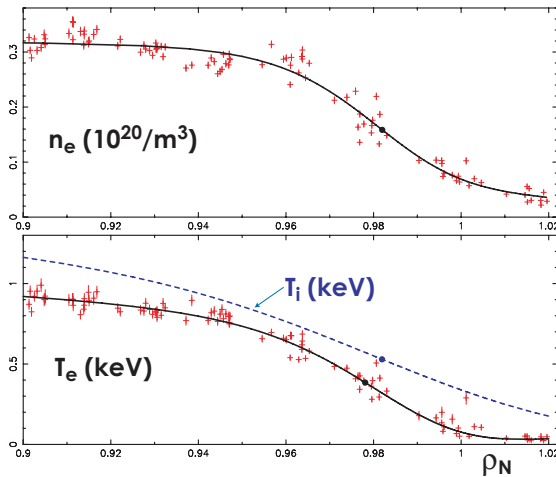


Figure 13: Edge pedestal n_e and T_e profiles for DIII-D shot 98889, averaged over 80–99% of time to next ELM crash, around 4500 ms.

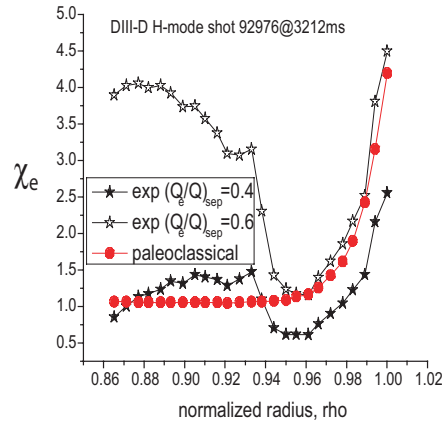


Figure 14: Transport analysis χ_e (m^2/s) in DIII-D pedestal depends on electron fraction of power flowing through separatrix, $(Q_e/Q)_{\text{sep}}$ [15].

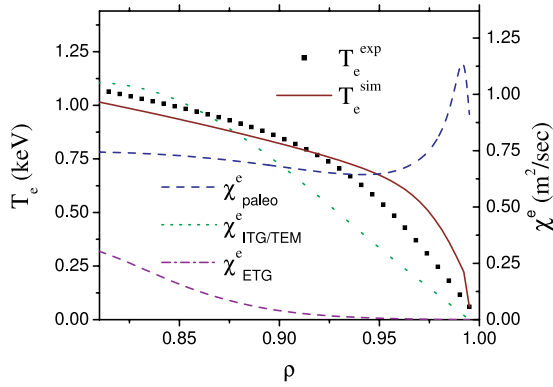


Figure 15: ASTRA modeling [16] of DIII-D edge $T_e(\rho)$ like in Fig. 13 with paleoclassical model.

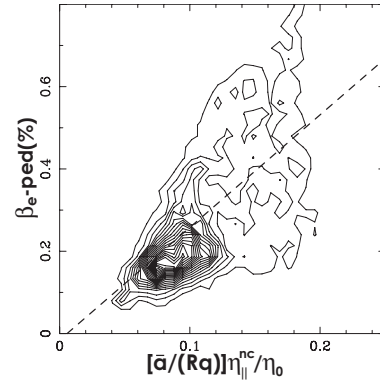


Figure 16: DIII-D database of β_e^{ped} (in %) versus β_e^{ped} paleoclassical parameter $(\bar{a}/R_0q)(\eta_{\parallel}^{\text{nc}}/\eta_0)$.

7. Non-tokamak Experiments: ST/NSTX, RFP/MST, Spheromak/SSPX

The paleoclassical model [1a,1c] applies to axisymmetric resistive, current-carrying toroidal plasmas of all types — spherical tokamaks (STs), reversed field pinches (RFPs), and spheromaks — in regions where $\epsilon^2, B_p^2/B_t^2 \ll 1$. Figure 17 shows that the paleoclassical model captures the decrease in core χ_e caused by moderately reversed shear ($q' < 0$ for $\rho < 0.45$) in an ohmic-level NSTX L-mode plasma, analogous to the $\rho < 0.6$ JT-60U results in Fig. 12. The dotted line in Fig. 17 indicates the region where the zero shear, $\max\{n_{\text{max}}\}$ formula at the end of (2) has been used. Figure 18 shows the ratio of the TRANSP analysis χ_e to the paleoclassical χ_e^{pc} at $\rho = 0.65$ for a variety L-mode NSTX discharges from the 2004 and 2005 campaigns. Two points about it are notable: 1) since all the data have ratios of about unity or greater the paleoclassical χ_e^{pc} is setting the irreducible minimum electron thermal diffusivity; and 2) χ_e is at the paleoclassical level for T_e less than about $0.65 B^{2/3}$ keV, but often above it for larger T_e . Similar comparisons for higher heating power NSTX H-modes [19] find that: the TRANSP χ_e usually significantly exceeds χ_e^{pc} throughout the plasma, their minimum ratio is never below 0.5, has a mean of about 4 and ranges up to 13; and all have $T_e/B^{2/3} \geq 0.5$ keV. Since for these NSTX discharges $\kappa \simeq 1.9$ and $\bar{a} \simeq 0.8$ m, this implies that for these discharges $T_e^{\text{crit}} \simeq (0.55\text{--}0.72) B^{2/3} \bar{a}^{1/2}$ keV, which is less than a factor of two smaller than (5) or alternatively indicates $f_{\#} \sim 1\text{--}2$.

For quiescent RFP plasmas such as those in MST PPCD discharges [20], the magnetic fluctuations due to tearing modes are reduced; thus, the magnetic-flutter-induced transport is reduced and the electron heat transport is reduced to tokamak levels. Figure 19 shows that the χ_e in these PPCD discharges is less than an order of magnitude above and has approximately the same shape as the paleoclassical χ_e^{pc} .

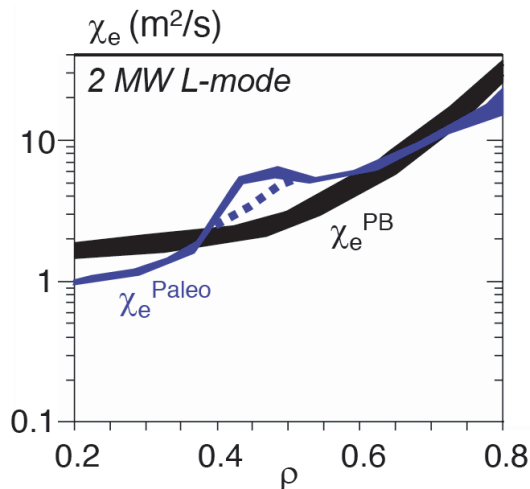


Figure 17: TRANSP and paleoclassical χ_e for an L-mode NSTX reversed shear plasma [19].

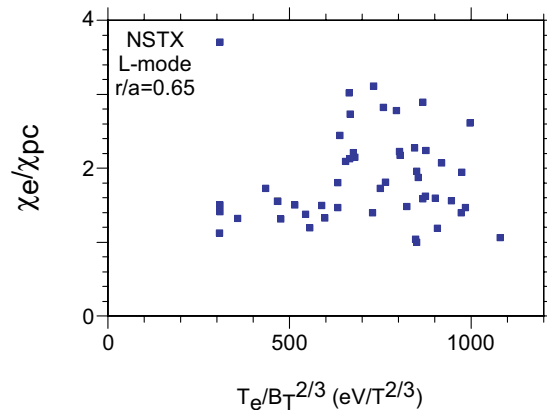


Figure 18: Ratio of TRANSP to paleoclassical χ_e versus $T_e/B_T^{2/3}$ parameter for NSTX L-modes.

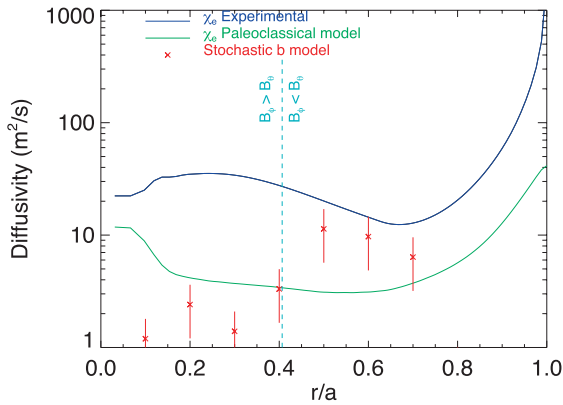


Figure 19: χ_e in quiescent (PPCD) MST plasmas [20]; transport is not below paleoclassical level.

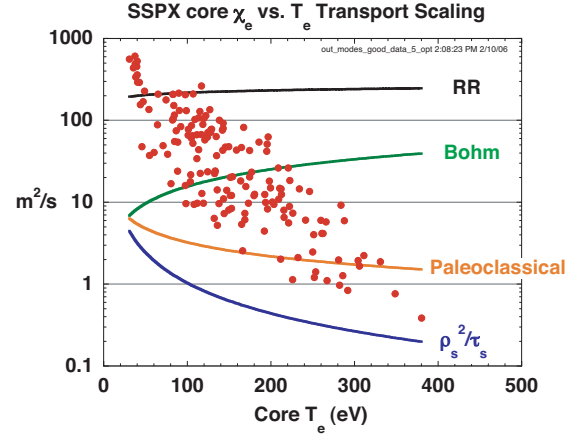


Figure 20: SSPX χ_e on axis decreases as T_e increases [21]; paleoclassical may limit at high T_e .

In the SSPX spheromak [21], as shown in Fig. 20, in $T_e \sim 100$ eV plasmas $n = 1$ magnetic fluctuations are present and produce a magnetic-flutter level χ_e (RR = Rechester-Rosenbluth). As T_e is increased (via magnetic flux increases), magnetic fluctuations and χ_e decrease. As indicated in Fig. 20, for $T_e \gtrsim 200$ eV the (collisional regime) paleoclassical χ_e^{pc} may set the lower limit on electron heat transport.

8. Conclusions About Paleoclassical Electron Heat Transport

From these studies, we conclude that paleoclassical transport may set the irreducible minimum (factor ~ 2) electron heat transport in many resistive, current-carrying toroidal plasmas — when not exceeded by fluctuation-induced transport due to RBMs for $T_e \lesssim 300$ eV in L-mode plasmas, drift-type microturbulence (ITGs, TEMs, ETGs) for $T_e \gtrsim T_e^{\text{crit}} \equiv B^{2/3} \bar{a}^{1/2} \text{keV}$ ($\sim 0.7\text{--}2.4$ keV in present devices but ~ 5 keV in ITER) or magnetic fluctuations (Rechester-Rosenbluth χ_e), or core ($\rho \lesssim 0.4$) sawtooth effects.

This research was supported by U.S. DoE grants and contracts DE-FG02-92ER54139 and DE-FC02-05ER54184 (UW-Madison), DE-FC02-04ER54698 (GA), DE-FG02-92ER54141 (Lehigh), DE-AC02-76CH03073 (PPPL), DE-FG02-99ER54512 (MIT), DE-AC05-00OR22725 (ORNL), W-7405-ENG-48 (LLNL), DE-FG02-00ER54538 (GaT-ech) and DE-FG02-99ER54523 (JHU). The JAEA work was supported by the Japan Society for the Promotion of Science. The FOM work was supported by the EC European Fusion Programme and NWO.

- [1] J.D. Callen, a) Nucl. Fus. **45**, 1120 (2005); b) PRL **94**, 055002 (2005); c) Phys. Plasmas **12**, 092512 (2005).
- [2] J.D. Callen, “Key hypothesis of paleoclassical model,” UW-CPTC 06-3, September 2006 (submitted to PoP).
- [3] Y. Camenen, A. Pochelon et al., Plasma Phys. Control. Fusion **47**, 1971 (2005) — see its Figure 10.
- [4] C.C. Petty, T.C. Luce et al., a) Nucl. Fusion **38**, 1183 (1998); b) Phys. Plasmas **6**, 909 (1999).
- [5] T.C. Arlen et al., GP1 36, DPP-APS Denver (2005); C.M. Greenfield et al., TTF Myrtle Beach, SC (2006).
- [6] B.A. Carreras, P.H. Diamond et al., PRL **50**, 503 (1983); B.N. Rogers, J.F. Drake et al., PRL **81**, 4396 (1998).
- [7] C.L. Rettig, T.L. Rhodes et al., Phys. Plasmas **8**, 2232 (2001); Plasma Phys. Control. Fusion **43**, 1273 (2001).
- [8] M.R. Wade, T.C. Luce, R.J. Jayakumar, P.A. Politzer, A.W. Hyatt et al., Nucl. Fusion **45**, 407 (2005).
- [9] E.A. Lazarus, F.L. Waelbroeck, T.C. Luce et al., Plasma Phys. Control. Fusion **48**, L65 (2006).
- [10] M. Greenwald, R.L. Boivin, F. Bombarda, P.T. Bonoli, C.L. Fiore et al., Nucl. Fusion **37**, 793 (1997).
- [11] a) N.J. Lopes Cardozo et al., PPCF **39**, B303 (1997); b) G.M.D. Hogewij et al., Nucl. Fus. **38**, 1881 (1998).
- [12] G.M.D. Hogewij, J.D. Callen, H.J. de Blank, “Paleoclassical Electron Internal Transport Barriers in RTP,” Controlled Fusion and Plasma Physics (Proc. 33th Eur. Conf., Roma, Italy, 2006), CD-ROM file P-4.148.
- [13] a) T. Fujita et al., Phys. Rev. Lett. **78**, 2377 (1997); b) Plasma Phys. Control. Fusion **46**, A35 (2004).
- [14] R. Nazikian, K. Shinohara, G.J. Kramer, E. Valeo et al., Phys. Rev. Lett. **94**, 135002-1 (2005).
- [15] W.M. Stacey and R.J. Groebner, Phys. Plasmas **13**, 072510 (2006).
- [16] A.Y. Pankin, G. Bateman, D.P. Brennan, D.D. Schnack, P.B. Snyder et al. Nucl. Fusion **46**, 403 (2006).
- [17] J.D. Callen, T.H. Osborne, W.M. Stacey, R.J. Groebner and M.A. Mahdavi, “Paleoclassical model for edge electron temperature pedestal,” UW-CPTC 06-6, October 2006 (to be published).
- [18] L.D. Horton, A.V. Chankin, Y.P. Chen, G.D. Conway, D.P. Coster et al., Nucl. Fusion **45**, 856 (2005).
- [19] D. Stutman, M.H. Redi, et al., “Studies of Improved Electron Confinement on NSTX” (to be published).
- [20] J.S. Sarff, J.K. Anderson, T.M. Biewer, D.L. Brower et al., Plasma Phys. Control. Fusion **45** A457 (2003).
- [21] H.S. McLean, R.D. Wood, B.I. Cohen, E.B. Hooper, D.N. Hill et al., Phys. Plasmas **13**, 056105 (2006).